THE JOURNAL OF PHYSICAL CHEMISTRY C
A JOURNAL OF THE AMERICAN CHEMICAL SOCIETY

pubs.acs.org/JPCC

Article

Molecular Dynamics Studies of the Melting Kinetics of Superheated Crystals

Jane HyoJin Lee,* Changho Kim,* and Michael E. Colvin

Cite This: https://doi.org/10.1021/acs.jpcc.1c10392

Read Online

ACCESS | Metrics & More | Article Recommendations | Supporting Information

ABSTRACT: Molecular dynamics (MD) simulations have long had an important role in the study of equilibrium and nonequilibrium phase transitions. However, the effects of finite system sizes and periodic boundary conditions on such simulation are still not fully understood. In the present paper, we investigate this issue using simulations of the homogeneous melting of superheated crystals, specifically the effect of system size on the delay time before melting (which we call "melting time"). Because melting is a random and relatively rare event, we perform a systematic and extensive MD simulation study of a simple molecular system, solid-phase argon in a perfect fcc crystal superheated above the melting point. Using extensive replicate simulations, we first confirm that the distribution of melting times is accurately characterized by a gamma distribution. Next, we use the model of melting being triggered by random dislocations to derive an equation for the mean melting time as a function of system size and show that this model well-matches our MD data over a range of periodic boxes containing from 256 to 296,352 argon atoms. This equation shows that the system-size effect is inversely proportional to the number of atoms (or equivalently, proportional to L^{-3} with L being the side length of the periodic box) and could be used as a correction factor for melting times calculated in finite systems. We also study the effects of temperature on melting and find that the mean melting time exponentially decreases to a nonzero asymptotic value with increasing temperature. We observe that the melting time distributions shift toward more Gaussian-like forms of the gamma distribution (i.e., with larger values of the shape parameter) at elevated temperatures. Finally, we also present the results of the melting of water ice I_h to show that our findings apply to molecules and melting processes more complex than simple Lennard-Jones systems.

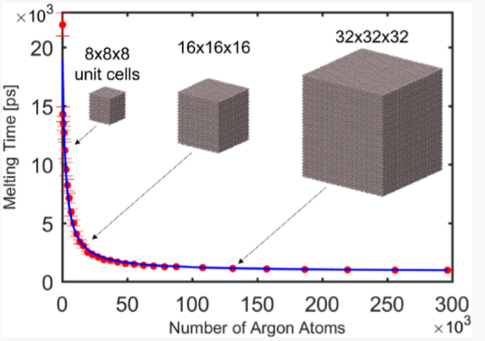

1. INTRODUCTION

Atomistic theories for melting date back over 100 years to Lindemann's melting theory[1] and this topic is still an area of active research.[2−4] Although these theories vary widely in their details and depend on whether the solid includes a surface or not (i.e., heterogeneous versus homogeneous melting), all involve a triggering step where one or a few atoms depart from their crystal site by more than a critical distance. These types of mechanisms, which have roots in Lindemann's melting criterion, have been validated by molecular dynamics (MD) simulations.[5−7] For example, an MD study of the superheated melting of Lennard-Jones crystals showed that melting can be triggered by the dislocation of as few as 5−6 atoms.[7]

As a complementary tool to pure theory, the MD simulation technique has been broadly used to study melting.[8] Thanks in part to the computational efficiency of periodic boundary conditions (PBCs), MD has been successfully employed to investigate homogeneous melting. Homogeneous melting is a nonequilibrium process observed from the defect-free superheated state. Due to difficulties in minimizing the effect of surfaces or grain boundaries, it is observed in experiments only under carefully chosen conditions[9] (e.g., metal spheres embedded into other metals having similar lattice constants). However, an infinite perfect crystal without surfaces can be readily modeled by MD using PBCs. In this setting, several simulation techniques have been developed to determine the melting temperature of a simulated material.[8,10,11] In the Z method,[12] where a sequence of microcanonical (*NVE*) ensemble MD simulations is performed, the maximum superheating is located using the criterion that the solid beyond the limit of superheating must melt into the liquid, and the melting pressure and temperature are determined as the pressure and temperature of the resulting liquid state at the maximum superheating. Although this method has the advantage of a simple simulation protocol and can be applied to relatively small systems, locating the maximum superheating can be inaccurate because the transition from the solid to the liquid is a rare event. In particular, as demonstrated by Alfè et

Received: December 7, 2021
Revised: February 2, 2022

al.,[13] the mean waiting time (until the transition occurs) becomes larger as the system size decreases or as the initial steady-state temperature of the solid decreases to the limit of superheating. Therefore, investigating the statistics of waiting times has not only theoretical importance to understanding the dynamical nature of the homogeneous melting process but also practical importance to the construction of a reliable computational procedure for determining melting points. Recently, by applying Bayesian statistical inference, Davis et al.[14] showed that the waiting time obeys a gamma distribution rather than an exponential distribution as previously asserted by Alfè et al.[13]

In the present paper, we investigate the kinetics of homogeneous melting beyond the limit of superheating. We focus on the distribution of the waiting time before melting (which we will simply call the "melting time"). The aim of the paper is twofold. First, we confirm that the distribution of melting times is accurately characterized by a gamma distribution and provide a theoretical model equation for the mean melting time based on the statistics of random atomic dislocation. Second, by estimating the two parameters of the gamma distribution, we investigate the dependence of the distribution of melting times on the system size as well as the system temperature. Precisely determining the distribution function of a physical quantity requires in general many more replicate values compared to calculating the moments (e.g., mean and variance) of the quantity. Furthermore, because the physical quantity of interest in the present paper, the melting time, arises from random and relatively rare events, a systematic and extensive MD simulation study is required. We created a very large data set of melting simulations to validate our theoretical model equation, which not only helps us understand the physics of melting but also enables us to concisely characterize the distribution of melting times for different system sizes and system temperatures. In this study, we use a simple system, solid-phase argon in a perfect fcc crystal superheated above the melting point. We also present the results of the melting of water ice I_h to show that our findings apply to molecules and melting processes more complex than simple Lennard-Jones systems.

Homogeneous melting has been investigated via the classical nucleation theory (CNT).[15−17] This has led to a theoretical framework to predict the maximum superheating achievable at various heating rates based on CNT and validated by MD simulations.[18−20] This approach focuses on when the first nucleus is formed and the rate of nucleus formation is related to the free energy of activation for the formation of the nuclei. This provides insight into the fundamental physics and thermodynamics of phase transitions. Our study explores how simulation parameters will influence the phase transition process observed in MD simulations. To this end, we investigate the distribution of melting times, which we define as the time until a global change due to melting occurs at superheated temperatures. This melting time is in contrast to the nucleation time determined by a local order parameter[21] because nuclei can form and disappear over a range of times. In this paper, we observe that these melting times are stochastic quantities whose distribution depends on the system size. We develop a systematic computational procedure to characterize the melting time distribution. As mentioned above, understanding the melting time distribution has practical importance to reliable determination of melting points using computational approaches. Hence, we believe that our computational study will give complementary information relevant to the CNT approach by providing reliable interpretation of the simulation results without relying on the free energy formulation.

For a physical quantity estimated by MD simulation, its dependence on the system size—the number of molecules in a single periodic image—is called the system-size effect. Accurate characterization and theoretical understanding of the system-size effect is crucial for reliable and computationally feasible MD simulations. When an infinite system is modeled by PBCs, several different types of pitfalls may arise.[22] For the equilibrium MD estimation of transport coefficients of simple fluids, such as self-diffusion coefficients[23] and shear viscosities,[24] the finite system-size corrections have been well established. However, the effects of PBCs can be subtle and complicated. For example, in the presence of long-range electrostatic interactions, the PBCs combined with the use of Ewald sums can even alter the ground-state conformation of small peptides.[25] The advent of supercomputers has allowed simulations large enough that some properties are effectively converged with respect to the size of the simulation box,[26] but simulations using complex force fields or requiring very long timescales or multiple replicates, are still run with PBC box sizes small enough to yield artifacts. The use of PBCs can also cause artifacts in simulations of equilibrium and nonequilibrium phase transition processes, including phase changes and related processes such as initial nuclei formation at the commencement of freezing.[27,28]

For equilibrium and nonequilibrium phase transition phenomena, several studies have made the distinction between PBC-induced artifacts versus the statistical effects of having more independent atoms in larger periodic boxes. For example, a 1990 study of the initial formation of pre-crystalline nuclei in supercooled Lennard-Jones liquid using periodic box sizes of 15,000 and 1,000,000 particles concluded that size effects were statistical, rather than a PBC-induced distortion of the results for the smaller periodic box.[29] That is, the larger box sampled a much larger number of independent configurations, allowing more opportunities for crystal nuclei to form. As mentioned above, Alfè et al. showed for superheated iron crystals that the mean melting time was inversely proportional to the number of atoms in the periodic box, consistent with melting being triggered by a rare event whose overall probability for the system increases with the number of independently moving atoms.[13] Another study that investigated the effects of the periodic box size on the time to melt for hard spheres using both kinetic Monte Carlo and MD simulations showed similar results.[30]

2. MD SIMULATIONS

We performed *NPT* (i.e., constant temperature and constant pressure) ensemble MD simulations of solid-phase argon superheated above the melting point for various system sizes and system temperatures. As mentioned in the Introduction, we performed a large number of replicate MD simulations (1000 to 2000 for most conditions, see below) to obtain an extensive data set of melting times for each value of system size and system temperature. Before providing the details of the MD simulations, we first describe the physical conditions under which those MD simulations were performed. We used as our initial state a highly compressed perfect fcc crystal with a density of 1.69 g/cm^3 and observed its melting process under 1 atm. To investigate the system-size effect on melting times, we

https://doi.org/10.1021/acs.jpcc.1c10392
J. Phys. Chem. C XXXX, XXX, XXX−XXX

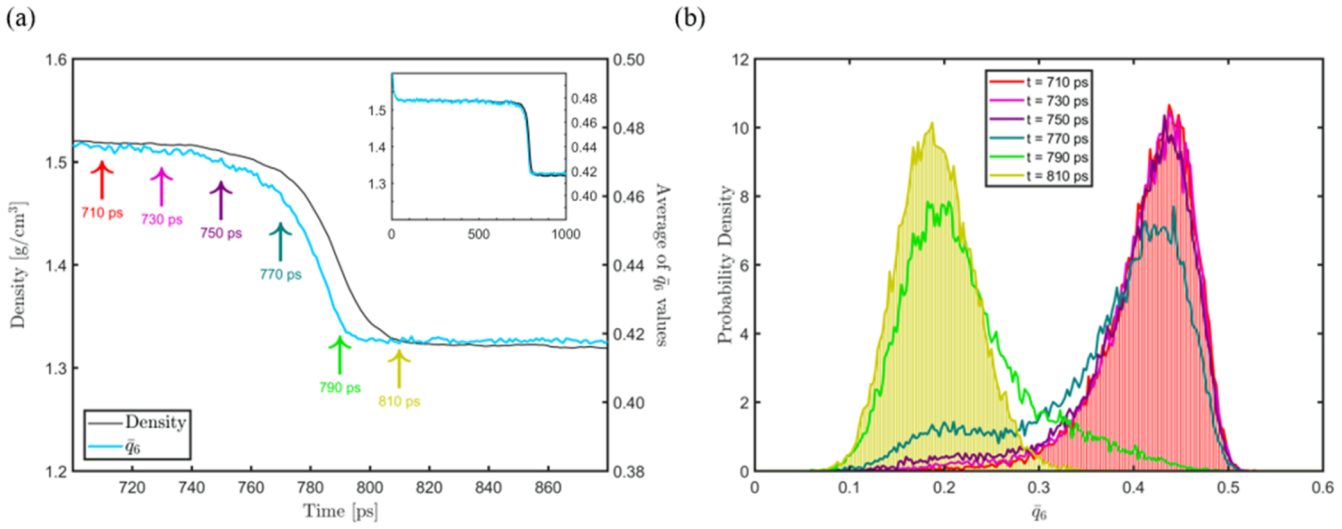

Figure 1. Changes of the system density and the local bond order parameter distribution during the melting process observed from an MD trajectory with $N = 20$ (i.e., $4N^3 = 32{,}000$ argon atoms). In the left panel, the time profile of the system density is superimposed with that of the average of the local bond order parameter values $\bar{q}_6$ (note that $\bar{q}_6$ is computed for each atom). In the inset, the two curves are shown for the entire simulation. In the right panel, the distributions of $\bar{q}_6$ values at chosen times are compared.

used a fixed temperature value $T = 99.5$ K. For the system temperature dependence, we used temperature values between 99.5 and 104 K. We chose the temperature values to be significantly higher than the melting point of 84.1 K at 1 atm so that melting times are not too long. The initial density of 1.69 g/cm^3 corresponds to solid argon under high pressure (~1080 atm) and experiments have shown that at this pressure argon has a melting point above 105 K[31] so that the initial, compressed system is stable as a solid over the temperature range we considered.

To capture the melting time of the argon crystal, we monitored the expansion of the system (during the *NPT* simulation) and then located the time when the density of the system first falls below a certain value (see Figure 1). From test calculations, we determined a good threshold value for the irreversible melting of the argon crystal to be 1.40 g/cm^3, which is close to the density of liquid argon, for example, 1.39 g/cm^3 at 87.3 K and 1 atm or 1.32 g/cm^3 at 99.5 K and 3 atm,[32] and considerably below the density of solid argon 1.62 g/cm^3 (at the triple point, 83.7 K and 0.68 atm).[33] We additionally verified that the midpoint in this rapid density change occurs at the same time as the peak of the spatial density fluctuations during melting, see Supporting Information Section 8.

To confirm that our density change criterion can reliably capture the time to irreversible melting, we compared the melting times estimated by this criterion with those estimated from the local bond order parameter distribution changes. To this end, we used the modified Steinhardt order parameter $\bar{q}_6$.[34] The definition of $\bar{q}_6$ and analysis results are given in Supporting Information Section 7. As shown in Figure 1, the melting times estimated from the density changes occur slightly later than those estimated from the order parameter. However, these time lags were observed to have consistent values around 10 ps. Given the similarity of the melting times determined using the order parameter and the density threshold, we opted to use the density criterion with our *NPT* simulations, which enabled us to obtain a very large number of replicate values of melting time in a computationally efficient manner. A more detailed discussion of our choice of *NPT* simulations is given in Supporting Information Section 6A. We note that *NPT* simulations have been used in several MD studies of homogeneous melting.[35−38]

To simulate a crystal of argon atoms, we used a Lennard-Jones forcefield, $V(r) = 4\varepsilon[(\sigma/r)^{12} - (\sigma/r)^6]$ with $\varepsilon = 0.9980$ kJ/mol and $\sigma = 0.3405$ nm. All simulations were performed using GROMACS version 5.0.7.[39] The initial states were different size periodic boxes of an fcc crystal containing $N \times N \times N$ unit cells (with N ranging from 4 to 42), yielding $M = 4N^3$ atoms in the periodic box. We created each initial periodic box of perfect fcc crystal with an initial density of 1.69 g/cm^3. We randomly initialized the atom velocities to a specified system temperature (between 99.5 and 104 K) and performed *NPT* simulation at 1 atm. We employed the Bussi velocity rescaling thermostat[40] with a time constant $\tau_T = 0.1$ ps and the Berendsen barostat[41] with a time constant $\tau_p = 1$ ps and a compressibility of 4.5×10^{-5} bar^{-1}. We ran test simulations with larger thermostat time constants (0.25, 0.5, and 1 ps) and found this had no effect on the melting time for periodic boxes with $N \geq 12$ ($M \geq 6912$ atoms). (See Supporting Information Section 6D for additional results and discussion on the thermostat time constant.) We used a 1 nm cutoff for the Lennard-Jones forces and a timestep of 2 fs. Due to its highly compressed initial structure, the system was observed to quickly expand to a density of ~1.52 g/cm^3 over a period of about 10 ps (see Supporting Information, Figure S11 of Supporting Information). After this change, the system was observed to maintain this density until the onset of melting. For more a detailed description of this initial behavior of the system, see Supporting Information Section 6B. To determine if our overall conclusions were dependent on this initialization procedure, we also tested starting the simulations from an ensemble of different initial structures with the argon atoms thermally dislocated from the perfect fcc crystal sites by sampling starting configurations from a short *NVE* simulation at the initial system volume, which yielded melting behavior similar to that obtained starting with a perfect fcc crystal (see Supporting Information Section 6C).

Simulations were performed for each replicate as a sequence of restarted short simulation segments (typically 500 ps in

https://doi.org/10.1021/acs.jpcc.1c10392
J. Phys. Chem. C XXXX, XXX, XXX−XXX

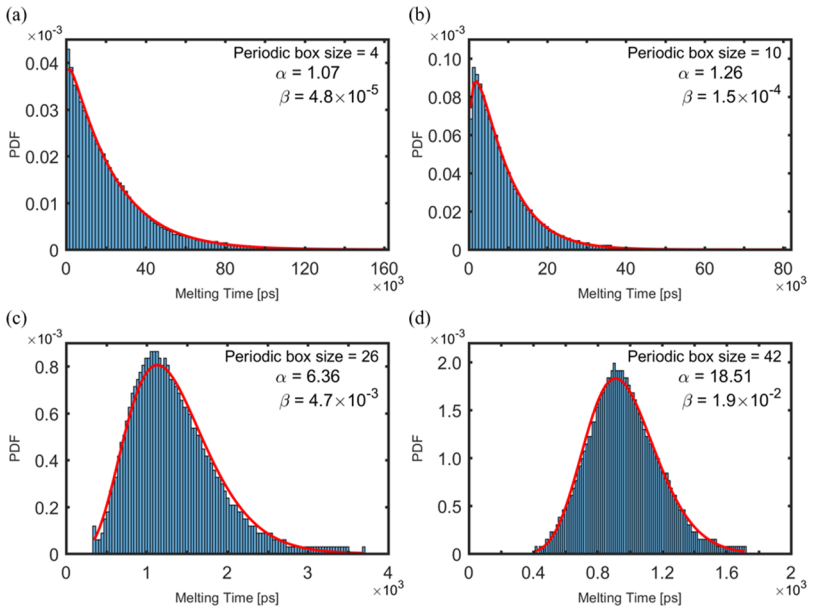

Figure 2. Gamma distribution fitted to the measured melting times for four different periodic box sizes at T = 99.5 K. The values of the α and β parameters are also shown. Each histogram has 100 bins and is smoothed with a moving average window of 15 bins. For periodic box size N, the number of argon atoms is $4N^3$.

length). The system density was calculated at the end of each segment and the simulation was restarted until the density value was below a critical level, indicating irreversible melting. The reported melting time for each replicate run was determined by scanning the densities for each frame in the trajectories and identifying the 1 ps interval when the density fell below 1.40 g/cm^3. The average and standard deviation of the melting times for each box size and temperature are given in Tables S1 and S2 of Supporting Information. These tables also include the average temperature of the system measured during the simulation to verify that there was no drift from the specified temperature. In addition to determining the melting times, for a subset of the replicate simulations, we calculated the radial distribution functions and the histograms of distances to the nearest neighbor atoms for the frozen portion of the trajectory (see Figure S3 of Supporting Information). As a validation of the accuracy of the energetics across the different periodic box sizes, we calculated the enthalpy of melting for one replicate for a range of box sizes at 99.5 K which yielded ΔH_{fus} = 1.122 ± 0.002 kJ/mol averaged over a selection of 26 box sizes, showing near identical results for all box sizes. This result is close to the experimental value of 1.19 kJ/mol[42] near the melting point of 83.8 K.

The system sizes and the numbers of replicate MD simulations used are as follows. For argon at T = 99.5 K, the initial states were 32 different sized periodic boxes containing $N \times N \times N$ cells for N = 4 to 27 and then 28 to 42 for even values of N, corresponding to a range of system sizes (denoted by the total number of argon atoms $M = 4N^3$) of 256 to 296,352 argon atoms (complete list is given in Table S1 of Supporting Information). For system sizes with N = 4 to 7, we performed 2000 replicate melting runs, that differed only in the initial random velocities used to set the system temperature. For system sizes with N = 8 to 42, we ran 1000 replicate melting runs. To determine the temperature dependence of the melting rates, we also ran simulations of argon melting for the range of temperatures from 100 to 104 K in half-degree units, for N = 4 to 9 (because larger simulation boxes would melt nearly instantly at elevated temperatures). For most higher-temperature simulations, we ran 200 replicates at each box size, except for the 100 K simulations for which we ran 800 replicates (complete list is given in Table S2 of Supporting Information).

In addition to argon melting simulations, we have also run water ice (I_h) melting simulations in the constant temperature and constant pressure ensemble for 11 different simulation box sizes at 281 K and 1 atm. The ice melting simulation is described in Supporting Information Section 5. The resulting averages and standard deviations of the melting times for all ice melting simulations are given in Table S5 of Supporting Information.

3. RESULTS AND DISCUSSION

In Section 3.1, we present our MD simulation results for the distribution of melting times and the dependence of this distribution on the system size. In Section 3.2, we present our theoretical model equation for the mean melting time as a function of system size and discuss the atomistic mechanism of homogeneous melting. In Section 3.3, we investigate the dependence of the melting time distribution on the system temperature, and in Section 3.4, we present MD simulation results for the melting of water ice.

3.1. Distribution of Melting Times and System-Size Dependence. In this section, using the large ensemble of melting times obtained from our MD simulations, we show that the melting times for the superheated argon crystals follow a gamma distribution. The gamma distribution

$$P(\tau) = \frac{\beta^{\alpha}}{\Gamma(\alpha)} \tau^{\alpha-1} e^{-\beta\tau} \qquad (\tau > 0)$$

describes the probability of the coincidental occurrences of independent events. Here, the shape parameter α is unitless and the rate parameter β has units of inverse time (specifically inverse picoseconds in our results). $\Gamma(\alpha) = \int_0^\infty x^{\alpha-1} e^{-x}\, dx$ is the gamma function.

https://doi.org/10.1021/acs.jpcc.1c10392
J. Phys. Chem. C XXXX, XXX, XXX−XXX

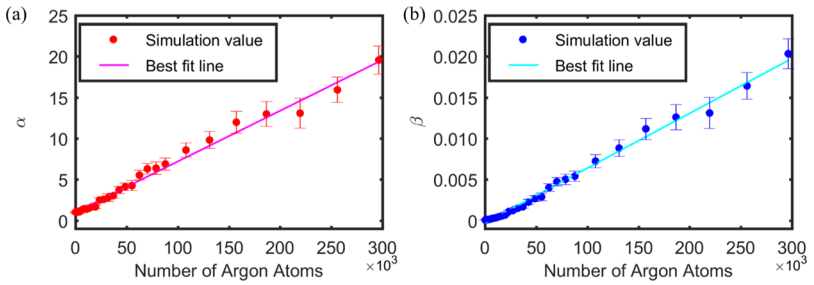

Figure 3. Plot of the α and β parameters of the gamma distribution versus the number of argon atoms in the periodic box at 99.5 K. The parameters were computed from the average and variance of the melting times across all replicates. The error bars were calculated from bootstrapping (see Supporting Information Section 3 for details.

For all replicates at each temperature and periodic box size, we calculated the time until melting occurred (as described in Section 2) to yield 200−2000 replicate melting times. Despite the large number of replicates, the resulting histograms were noisy (see Figure S1 of Supporting Information), so we performed a smoothing procedure on the histograms. To optimize the bin width and averaging window, we calculated 22 different histograms for each set of data by varying the number of bins between 20 and 150. Then, for each different histogram, we applied a (uniformly weighted) moving average smoothing filter with nine different window sizes. For the full list of the number of bins and the width of moving average window, see Table S3 of Supporting Information. In this way, we determined it was best to use 100 bins in the histograms and a moving average window of 15 bins for the smoothing procedure.

The resulting smoothed histograms for periodic box sizes N = 4, 10, 26, and 42 are shown in Figure 2. (See Figure S1 of Supporting Information for the unsmoothed histograms for the same periodic box sizes.) By comparing histograms of the melting times for the different box sizes, we observe that the melting time follows an exponential distribution for the smallest periodic box size and this transitions to a Gaussian distribution for the largest box size. Because the gamma distribution becomes an exponential distribution in the limit $\alpha \to 1$ and converges to a Gaussian distribution for large α, this observation suggests that the melting times for all of the systems may follow gamma distributions with different values of the α and β parameters. Hence, we fitted the (smoothed) histograms to the gamma distribution to determine the best fit values for the parameters α and β. Figure 2 clearly shows that each histogram is well described by a gamma distribution with the fitted values of α and β.

To further corroborate that the melting times for the superheated argon crystals follow a gamma distribution, we perform a chi-squared test as follows. For each periodic box size, we tested whether the smoothed distribution data comes from a gamma distribution using the chi-square goodness-of-fit test.[43] This calculates a test statistic (p-value) that is essentially the probability of getting the observed distribution of melting times if the data follows a gamma distribution. In other words, the null hypothesis is that the data is from a gamma distribution. For all periodic box sizes tested, the p-values were very large ($0.92 < p < 1$).

We note that our results are consistent with the recent MD study by Davis et al.,[14] where argon crystals in a 500-atom periodic box were superheated to extremely high temperatures leading to very short waiting times of <50 ps. Compared with that study, our results were obtained at much lower temperatures and for much larger periodic box sizes. It is perhaps not surprising that the gamma distribution arises for melting rates because it describes the probability of the coincidental occurrences of independent events and would be consistent with melting being triggered by a critical number of simultaneous atomic dislocations in the argon crystal. Though the lognormal, Weibull, and gamma distributions have been frequently used to model random times owing to their flexibility to fit empirical positive-valued distributions using their multiple parameters, the gamma distribution is well suited to model a random time that can be related to the occurrences of independent events. In particular, the Erlang distribution is a special case of the gamma distribution when α is an integer value and predicts the waiting time until the α-th event occurs for independent events with the same rate β. In addition, the gamma distribution family includes the exponential distribution as well as the normal distribution as its limiting cases, which also justifies our choice based on the simulation results. Interestingly, the gamma distribution arises in several descriptions of energy and atomic fluctuations as well as the rates of nonequilibrium processes. This distribution has been found to describe the energy distributions in both NVT[44] and NVE[45] ensembles. In another example, the use of a modified (shifted) gamma distribution to describe atomic fluctuations in proteins was found to best fit neutron scattering data.[46] Finally, an MD study of the gas−liquid nucleation rates during the condensation of a Lennard-Jones gas found that the gamma distribution described the nucleation onset times for several MD thermostats tested.[47]

Under the assumption that the melting times follow a gamma distribution, the α and β parameters can be more easily estimated using the mean μ and variance σ^2 of the melting times (i.e., without computing and fitting the histogram) and using the relations

$$\alpha = \frac{\mu^2}{\sigma^2}, \qquad \beta = \frac{\mu}{\sigma^2}$$

Figure 3 shows that the estimated values of α and β for the system temperature of 99.5 K increase as the system size increases. For the number of argon atoms in the periodic box, denoted by M, the parameters α and β are reasonably well described by the following linear expressions obtained by linear regression: $\alpha = 6.2 \times 10^{-5}M + 1.0$ ($R^2 = 0.989$) and $\beta = 6.7 \times 10^{-8}M - 3.1 \times 10^{-4}$ ($R^2 = 0.994$). The error bars on the α and β values were calculated using bootstrapping as described in Supporting Information Section 3. We note that there appears to be a slight bend in the curve for larger box sizes, but the data is too noisy to rule out a simple linear fit. Finally, as a validity check for our numerical procedures for calculating α and β,

https://doi.org/10.1021/acs.jpcc.1c10392
J. Phys. Chem. C XXXX, XXX, XXX−XXX

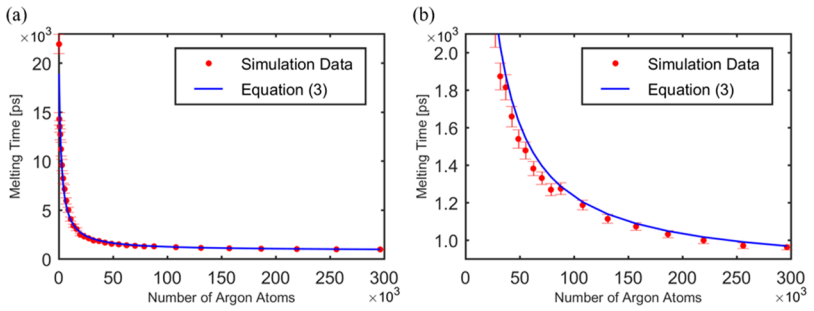

Figure 4. Plot of the melting time μ_M vs the number of argon atoms (M) in the periodic box. For the system temperature of 99.5 K, results from all 32 different periodic box sizes are shown in panel (a). The same but zoomed-in plot is drawn in panel (b). Filled red circles with error bars corresponding to two standard deviations denote the MD simulation results, whereas blue solid lines denote the fitted curve to eq 3.

these linear fits were also computed using the parameter values determined by fitting to the smoothed histograms, and the resulting slopes of the linear regression results for α and β varied by only 8.6 and 6.5%, respectively.

The linear expression of α with the intercept value close to 1 (i.e., $\alpha \approx 1$ at $M = 0$) is consistent with our observation made in Figure 2 that the distribution of melting times is close to an exponential distribution for small system sizes and it approaches a Gaussian distribution for large system sizes. Despite the negative intercept given in the linear expression of β, the actual value of the rate parameter β smoothly asymptotes to 0 for small values of M. Based on these two observations, we express $\alpha = a_0 + a_1 M$ and $\beta = bM$, which give the following expression for the mean melting time $\mu_M = \alpha/\beta$ of the system size M

$$\mu_M = \frac{a_0}{b}\cdot\frac{1}{M} + \frac{a_1}{b} \tag{1}$$

Hence, the MD simulation results suggest that the system-size effect on the mean melting time is inversely proportional to the number of atoms M. Equivalently, the system-size effect is proportional to L^{-3} with L being the side length of the periodic box. We note that this M^{-1} (or L^{-3}) dependence is different from that seen for transport coefficients such as the self-diffusion constant, which has a periodic box size correction factor proportional to $M^{-1/3}$ (or L^{-1}).[23] In the next section, we will develop a theoretical model that explains the M^{-1} dependence of the system-size effect of the mean waiting time and further investigate the validity of relation (1) using MD simulation results.

In addition to the mean melting time, we also studied the variance (σ_M^2) in the melting times, which we find also decrease in an approximately inverse relationship with M, as shown in Figure S2 of Supporting Information. This relation can be expressed as

$$\sigma_M^2 = \frac{\alpha}{\beta^2} = \frac{a_0 + a_1 M}{b^2 M^2} \approx \frac{a_1}{b^2}\cdot\frac{1}{M}$$

3.2. Theoretical Model Equation for Mean Melting Time.

In this section, we derive a model equation for the mean melting time by assuming that melting is initiated by one or a group of atoms simultaneously moving due to thermal motion a significant distance away from their equilibrium position in the lattice. We introduce a parameter m ($1 \le m \ll M$) which is the number of atoms that need to be simultaneously displaced to commence melting. We also introduce the probability q ($0 < q \ll 1$) that such a group of atoms moves far enough away from the equilibrium position to trigger melting during some time interval Δt. Then, the probability that at least one group has sufficient dislocation during Δt is given as $1 - (1 - q)^{M/m}$. We note that this probability converges to unity as M increases. Because the mean melting time is inversely proportional to this probability, we have a system-size dependent term $\Delta t/[1 - (1 - q)^{M/m}]$. In the limit of very large system sizes ($M \to \infty$) this term converges to Δt, indicating that the necessary dislocations to trigger melting will happen in the first time interval with 100% probability. Assuming that there is a finite delay between the triggering dislocations and the overall change in the system's density, we define this delay time as μ_∞, which will be the average melting time of an infinitely large periodic box. Overall, the average time until a crystal with a periodic box containing M atoms melts is given as

$$\mu_M = \frac{\Delta t}{1 - (1 - q)^{(M+c)/m}} + \mu_\infty \tag{2}$$

Note that we have included an offset parameter c to M, which we empirically found necessary to best describe the results for small systems.

Because we assume q is small, we can simplify eq 2 to

$$\mu_M \approx \frac{\Delta t \frac{m}{q}}{M + c} + \mu_\infty \tag{3}$$

Simplifying steps are shown in Supporting Information Section 1. We note that eq 3 (without the empirical offset parameter c) has the same form as eq 1, which was obtained from the MD simulation results. This agreement implies that the system-size effect observed in the MD simulations is due to the statistical effects of having more independent atoms in larger periodic boxes rather than PBC-induced artifacts.

Using eq 3, one can not only determine μ_M as an explicit function of M by fitting the MD results but also interpret the values of the fitting parameters from the microscopic viewpoint. In this paper, we use $\Delta t = 1$ ps, which is the timestep size used for monitoring melting in our MD simulations. Fitting eq 3 to the mean melting times of different system sizes for the system temperature 99.5 K yields $\mu_\infty = 832$ ps, $m/q = 4.083 \times 10^7$, and $c = 2.002 \times 10^3$ with the R^2 coefficient value of 0.97. The MD simulation results and the fitted curve are shown in Figure 4. The μ_∞ value is the mean melting time for a simulation using an infinitely large simulation box at 99.5 K. As described in Section 3.3, this asymptotic value is strongly dependent on the system temperature. The value of m/q is the inverse of the probability per atom of a melting-inducing fluctuation occurring during $\Delta t = 1$ ps. The c parameter determines the asymptotic melting

https://doi.org/10.1021/acs.jpcc.1c10392
J. Phys. Chem. C XXXX, XXX, XXX−XXX

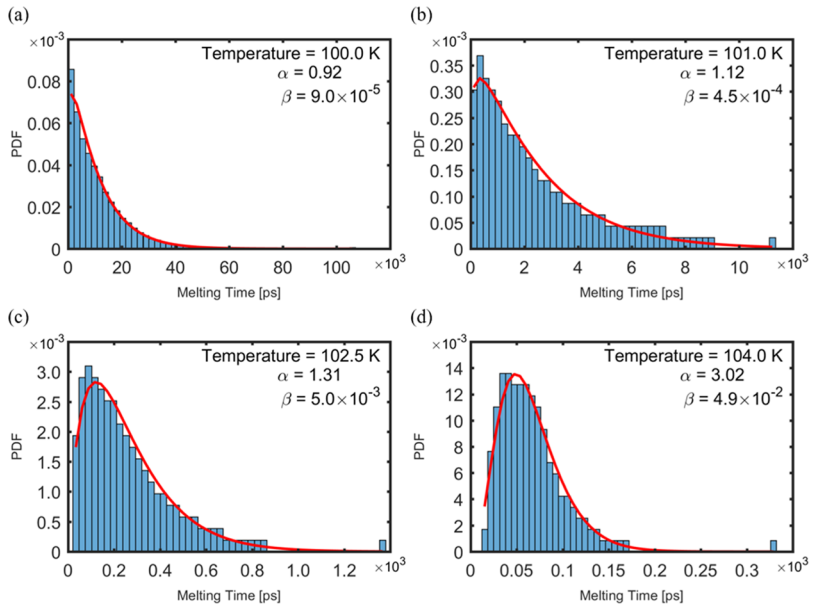

Figure 5. Gamma distribution fitted to the measured melting times for the periodic system containing 256 argon atoms at four different temperature values T = 100, 101, 102.5, and 104 K. The values of the α and β parameters are also shown.

time as the size of the periodic box becomes very small. The observed inverse relationship given in eq 3 suggests a practical way to correct for finite size effects in simulations of melting times and similar properties by running the simulation with different sized periodic boxes and extrapolating to infinite box size using this equation.

As mentioned above, the preceding analysis proposes that the inverse relationship between the mean melting time and the size of the periodic box is entirely due to the change in the number of independently moving argon atoms. Another possible explanation would be that different periodic box sizes lead to structural differences in the frozen crystal that are more stable for smaller periodic boxes. To investigate this possibility, we calculated and plotted the radial distribution functions and nearest-neighbor distances during the frozen portion of the trajectory for selected T = 99.5 K replicates for all periodic box sizes. The plots in Figure S3 of Supporting Information show that for both of these distance measurements, the lines for all replicates of all periodic box sizes are well superimposed. This shows that there are no large differences in the crystal structures for the different box sizes causing differences in the melting times.

3.3. Temperature Dependence. In this section, using the additional melting simulation results for higher temperatures (T = 100, 100.5, ..., 104 K), we investigate the temperature dependence of the statistics of melting times and analyze the thermodynamics of the transition. Because the higher-temperature simulations melt much faster than the 99.5 K runs, we limited MD simulations to the six smallest periodic boxes. The average and standard deviation of the melting times for 9 different temperatures are given in Table S2 of Supporting Information.

We first confirm whether the observations made for the 99.5 K simulations hold for the elevated temperatures. As shown in Figure 5, the distribution of melting times follows a gamma distribution for each temperature. Additionally, at each temperature, nearly linear relationships are observed between the gamma distribution parameters and the size of the periodic box (see Figure S4 of Supporting Information) as observed for 99.5 K (see Figure 3). We also confirm the M^{-1} dependence of the system-size effect of the mean melting time μ_M for each temperature (see Figure S5 of Supporting Information) as for 99.5 K (see Figure 4).

Next, we investigate the temperature dependence for these results. By comparing the distributions for higher temperatures shown in Figure 5 to the one for 99.5 K with the same system size M = 256 (see Figure 2a), we observe that the distributions are shifted to shorter average melting times at higher temperatures and that the distributions look more like Gaussian distributions with increasing temperature. These observations imply that both parameters α and β increase as the system temperature increases (note that $\beta = \alpha/\mu$ increases because α increases and μ decreases with T). For different system sizes, this behavior of α and β is shown in Figure S6 of Supporting Information, where we find that the growth is much faster than linear for both α and β as the temperature is increased. This temperature dependence of the α and β parameters can also be seen from the aforementioned linear relationships between these coefficients and the number of argons in the periodic box (shown in Figure S4 of Supporting Information). The slopes of these linear relationships increase with temperature.

To summarize, these results show an interesting interrelationship between the system size, the temperature, and the resulting gamma distribution parameters α and β. As we discussed previously, at 99.5 K, these parameters increase linearly with the number of atoms, so that the largest systems have melting time distributions that are nearly Gaussian, and the smallest systems have exponential melting time distributions. Likewise, increasing the temperature increases the distribution parameters, so that small, hotter systems have gamma distribution parameters similar to much larger systems at lower temperatures. For example, a system with 256 atoms at 104 K has nearly the same α parameter value (α = 3.02) as a system with 37,044 atoms at 99.5 K (α = 3.01). A similar trend is seen for the β parameter: β = 0.023 for 256 atoms at 103.5 K and β = 0.020 for 296,352 atoms at 99.5 K. In all cases, the changes that decrease the melting time, either increasing the

https://doi.org/10.1021/acs.jpcc.1c10392
J. Phys. Chem. C XXXX, XXX, XXX−XXX

system size or raising the temperature, lead to a more Gaussian-like distribution, and changes that increase the melting time, lead to a more exponential-like distribution. Results for the temperature dependence of the fitted parameters in eq 3 are described in Supporting Information Section 4.

We now analyze the thermodynamics of the melting process using the simulation data. Early theoretical models of melting processes led to the following form of expressions for the rate of nucleation (the collection of dislocations leading to melting)

$$\text{rate} = AT\ e^{-\Delta E^*/k_B T}$$

where A is the reaction prefactor, k_B is the Boltzmann constant, and ΔE^* is the activation energy for the reaction.[48] One challenge in computing a reaction rate from our measured average melting time is that a proper rate should be based on the time at which the process first reaches the top of the reaction barrier. However, melting times determined by the procedure described in Section 2 are expected to have a positive bias. To determine the correct time offset, we assumed that the rate is obtained as the reciprocal of the adjusted time $\mu_M - t_{offset}$

$$\text{rate} = \frac{1}{\mu_M - t_{offset}}$$

Then, we optimized the value of t_{offset} to maximize the R^2 value when fitting the computed rate data to the logarithm of the rate expression

$$\ln(\text{rate}) = \ln(A) + \ln(T) - \frac{\Delta E^*}{k_B}\left(\frac{1}{T}\right)$$

Because the value of $\ln(T)$ is nearly constant over our range of temperatures (99.5−104 K), we noted that the fit to this equation is essentially indistinguishable from a fit to the Arrhenius equation, that is

$$\ln(\text{rate}) = \ln(\bar{A}) - \frac{\Delta E^*}{k_B}\left(\frac{1}{T}\right)$$

Thus, we computed linear regression using the latter equation (i.e., instead of computing nonlinear fitting to the former equation). For each of the five smallest periodic box sizes, we performed the optimization procedure using 10 temperature points. The plots of the resulting fits are given in Figure 6. The optimized t_{offset} values and the corresponding fitting results are given in Table S4 of Supporting Information. We note that the optimized values of $t_{offset} \approx 30$ ps are similar across different system sizes. Considering that the magnitude of μ_M significantly varies depending on the system size, these consistent values strongly support our use of t_{offset}. In addition, all fits have good R^2 values (all greater than 0.98).

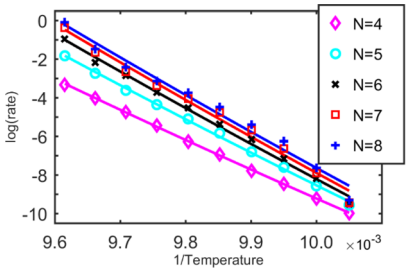

Figure 6. Plot of the logarithm of the rate, $\ln(rate)$, vs the inverse temperature, T^{-1}, for the five smallest periodic box sizes. N denotes the number of unit cells in each direction. Solid lines depict the linear regression results.

The predicted activation energies ΔE^* increase with the size of the periodic box, from 127.82 kJ/mol for $N = 4$ to 159.48 kJ/mol for $N = 8$. Because the interatomic potential is very short-ranged, the energy to dislocate an atom by a fixed distance in the frozen crystal lattice should not depend on the size of the periodic box. Therefore, the predicted lower activation barrier for the smaller periodic boxes indicates that melting can be achieved with less dislocation than in the larger boxes. This makes sense because for the smaller box there will be nearby dislocations in each surrounding periodic image.

The smaller boxes have lower activation energies yet have an overall lower melting rate than the larger boxes. Their slower rate is due to their lower prefactors: $\ln \bar{A} = 144.50$ for $N = 4$ compared with $\ln \bar{A} = 184.15$ for $N = 8$. In conventional chemical reactions, the prefactor (which is also known as the "frequency factor") describes the frequency at which collisions occur with sufficient energy for a reaction to occur. In our case, the prefactor is proportional to the rate of argon fluctuations that are sufficiently large to cause the crystal to melt.

3.4. Melting of Water Ice. The melting time data from the water ice simulations (described in Supporting Information Section 5) were analyzed using the same approach we applied to argon melting. We observed that the gamma distribution parameters, α and β, follow a linear relationship with M (see Figure S10 of Supporting Information) like the argon melting data we showed in Figure 3. We also confirmed that the measured average melting times (μ_M) versus the number of water molecules (M) is well described by eq 3. Figure 7 shows

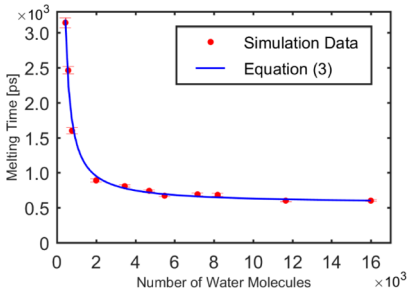

Figure 7. Plot of the melting time μ_M vs the number of water molecules (M) in the periodic box. For the ice system at 281 K, results from 11 different periodic box sizes are shown. Filled red circles with error bars corresponding to two standard deviations denote the MD simulation results, whereas the blue solid line denotes the fitted curve to eq 3. The values of the fitting parameters are $\mu_\infty = 556$ ps, $m/q = 7.3 \times 10^5$, and $c = -155$.

that the melting time follows an approximately inverse relationship with the size like the argon melting time (see Figure 4) and the melting time asymptotes to a fixed value (μ_∞) which is the predicted melting time for an infinitely large periodic box at 281 K.

4. CONCLUSIONS

PBCs are a purely artificial construct to imitate "macroscopic" experimental samples using dramatically smaller "microscopic" systems (rarely greater than 10^9 atoms and usually much smaller) that are amenable to simulation. In addition to the documented artifacts of PBCs that can arise when calculating equilibrium properties, for simulations of equilibrium and

https://doi.org/10.1021/acs.jpcc.1c10392
J. Phys. Chem. C XXXX, XXX, XXX−XXX

nonequilibrium phase transition processes, the size of the periodic box adds an additional artifact due to the limited number of independent particles whose random motion can trigger phase transition. In this study, we used the model problem of the melting of superheated argon ice crystals to demonstrate that the resulting system-size effect of the mean melting time is inversely proportional to the number of atoms in a periodic box. To corroborate this system-size effect, we derived eq 3 for the mean melting time, which involves the rate of melt-inducing spontaneous dislocations in the crystal, $q/(m\Delta t)$, and the asymptotic average melting time for an infinitely large periodic box, μ_∞. After confirming that the distribution of melting times follows the gamma distribution, we also investigated the behavior of the shape (α) and rate (β) parameters of the distribution to characterize the interrelationship between the system size, the temperature, and the melting time distribution. Both parameters increase linearly with the number of atoms in the periodic box. Though the resulting dependence of the mean melting time on the periodic box size is seen at all temperatures studied, the effect is shifted so that the melting time distribution for smaller periodic boxes at a particular temperature is similar to that for larger periodic boxes at lower temperatures. More specifically, the changes that decrease the melting time, either increasing the system size or raising the temperature, lead to a more Gaussian-like distribution, whereas changes that increase the melting time, lead to a more exponential-like distribution. The subsequent analysis of the rate kinetics of the melting process for different system sizes showed that the activation energy is higher for larger boxes, but this is more than offset by the increase in the prefactor for larger boxes, leading to a net increase in melting rates for larger boxes. In practical terms, this study shows that simulations of phase transition processes in systems using PBCs should be corrected by running the simulation with different size periodic boxes and extrapolating to infinite box size.

■ ASSOCIATED CONTENT

Supporting Information

The Supporting Information is available free of charge at https://pubs.acs.org/doi/10.1021/acs.jpcc.1c10392.

Derivation of eq 3 for the mean melting time; summary of the argon melting simulation results for 99.5 K and higher temperatures; additional plots for the argon melting simulations at 99.5 K; additional plots and discussion for the argon melting simulations at elevated temperatures; summary of ice melting simulations; results supporting the choices of simulation ensemble, initialization process, and thermostat time constant; local bond order parameter analysis; and spatial density fluctuations during the melting process (PDF)

■ AUTHOR INFORMATION

Corresponding Authors

Jane HyoJin Lee − *Department of Mathematics, Stonehill College, Easton, Massachusetts 02357, United States;* orcid.org/0000-0003-0260-8602; Email: jlee7@stonehill.edu

Changho Kim − *Department of Applied Mathematics, University of California, Merced, California 95343, United States;* orcid.org/0000-0002-4064-8237; Email: ckim103@ucmerced.edu

Author

Michael E. Colvin − *Department of Chemistry and Biochemistry, University of California, Merced, California 95343, United States*

Complete contact information is available at: https://pubs.acs.org/10.1021/acs.jpcc.1c10392

Notes

The authors declare no competing financial interest.

■ ACKNOWLEDGMENTS

The authors gratefully acknowledge computing time on the Extreme Science and Engineering Discovery Environment (XSEDE), which was supported by National Science Foundation grant no. ACI-1053575, and the Multi-Environment Computer for Exploration and Discovery (MERCED) cluster at UC Merced, which was funded by National Science Foundation grant no. ACI-1429783. J.L. was partially supported by the Stonehill College Conboy Award for Faculty Development program, C.K. was partially supported by the UC Merced Academic Senate Faculty Research Grants program, and M.E.C. was partially supported by the Art and Fafa Kamangar Chair in Biological Science at UC Merced. In addition, J.L. acknowledges two students, Nicolas M. Cannavo Berrazueta and Jaisil Chacko (2020 Stonehill College graduates) who participated in the summer research project, SURE 2018, and worked on the initial ice melting simulations. C.K. acknowledges Indar Freitas (UC Merced undergraduate student) who performed the local bond order parameter analysis as part of his undergraduate research supported by National Science Foundation Research and Training Grant no. DMS-1840265.

■ REFERENCES

(1) Lindemann, F. A. The Calculation of Molecular Vibration Frequencies. *Phys. Z.* **1910**, *11*, 609−612.

(2) Samanta, A.; Tuckerman, M. E.; Yu, T.-Q.; E, W. Microscopic Mechanisms of Equilibrium Melting of a Solid. *Science* **2014**, *346*, 729−732.

(3) Pedersen, U. R.; Costigliola, L.; Bailey, N. P.; Schrøder, T. B.; Dyre, J. C. Thermodynamics of Freezing and Melting. *Nat. Commun.* **2016**, *7*, 12386.

(4) Vopson, M. M.; Rogers, N.; Hepburn, I. The Generalized Lindemann Melting Coefficient. *Solid State Commun.* **2020**, *318*, 113977.

(5) Jin, Z. H.; Gumbsch, P.; Lu, K.; Ma, E. Melting Mechanisms at the Limit of Superheating. *Phys. Rev. Lett.* **2001**, *87*, 55703.

(6) Delogu, F. Mechanistic Aspects of Homogeneous and Heterogeneous Melting Processes. *J. Phys. Chem. B* **2006**, *110*, 12645−12652.

(7) Belonoshko, A. B.; Davis, S.; Skorodumova, N. V.; Lundow, P. H.; Rosengren, A.; Johansson, B. Properties of the Fcc Lennard-Jones Crystal Model at the Limit of Superheating. *Phys. Rev. B: Condens. Matter Mater. Phys.* **2007**, *76*, 64121.

(8) Alavi, S.; Thompson, D. L. Simulations of Melting of Polyatomic Solids and Nanoparticles. *Mol. Simul.* **2006**, *32*, 999−1015.

(9) Wang, Z.; Wang, F.; Peng, Y.; Han, Y. Direct Observation of Liquid Nucleus Growth in Homogeneous Melting of Colloidal Crystals. *Nat. Commun.* **2015**, *6*, 6942.

(10) Zhang, Y.; Maginn, E. J. A Comparison of Methods for Melting Point Calculation Using Molecular Dynamics Simulations. *J. Chem. Phys.* **2012**, *136*, 144116.

(11) Wang, S.; Zhang, G.; Liu, H.; Song, H. Modified Z Method to Calculate Melting Curve by Molecular Dynamics. *J. Chem. Phys.* **2013**, *138*, 134101.

(12) Belonoshko, A. B.; Skorodumova, N. V.; Rosengren, A.; Johansson, B. Melting and Critical Superheating. *Phys. Rev. B: Condens. Matter Mater. Phys.* **2006**, *73*, 12201.
(13) Alfè, D.; Cazorla, C.; Gillan, M. J. The Kinetics of Homogeneous Melting beyond the Limit of Superheating. *J. Chem. Phys.* **2011**, *135*, 024102.
(14) Davis, S.; Loyola, C.; Peralta, J. Bayesian Statistical Modeling of Microcanonical Melting Times at the Superheated Regime. *Phys. A* **2019**, *515*, 546−557.
(15) Christian, J. W. *The Theory of Transformations in Metals and Alloys*; Pergamon: Oxford, 2002.
(16) Motorin, V. I.; Musher, S. L. Kinetics of the Volume Melting. Nucleation and Superheating of Metals. *J. Chem. Phys.* **1984**, *81*, 465−469.
(17) Kelton, K. F. Crystal Nucleation in Liquids and Glasses. In *Solid State Physics*; Ehrenreich, H., Turnbull, D., Eds.; Academic Press, 1991; Vol. *45*, pp 75−177.
(18) Luo, S.-N.; Ahrens, T. J. Superheating Systematics of Crystalline Solids. *Appl. Phys. Lett.* **2003**, *82*, 1836−1838.
(19) Luo, S.-N.; Ahrens, T. J.; Çağın, T.; Strachan, A.; Goddard, W. A.; Swift, D. C. Maximum Superheating and Undercooling: Systematics, Molecular Dynamics Simulations, and Dynamic Experiments. *Phys. Rev. B: Condens. Matter Mater. Phys.* **2003**, *68*, 134206.
(20) Luo, S.-N.; Strachan, A.; Swift, D. C. Nonequilibrium Melting and Crystallization of a Model Lennard-Jones System. *J. Chem. Phys.* **2004**, *120*, 11640−11649.
(21) Radhakrishnan, R.; Trout, B. L. Order Parameter Approach to Understanding and Quantifying the Physico-Chemical Behavior of Complex Systems. In *Handbook of Materials Modeling*; Yip, S., Ed.; Springer Netherlands: Dordrecht, 2005; pp 1613−1626.
(22) Frenkel, D. Simulations: The Dark Side. *Eur. Phys. J. Plus* **2013**, *128*, 1−41.
(23) Yeh, I.-C.; Hummer, G. System-Size Dependence of Diffusion Coefficients and Viscosities from Molecular Dynamics Simulations with Periodic Boundary Conditions. *J. Phys. Chem. B* **2004**, *108*, 15873−15879.
(24) Kim, K.-S.; Kim, C.; Karniadakis, G. E.; Lee, E. K.; Kozak, J. J. Density-Dependent Finite System-Size Effects in Equilibrium Molecular Dynamics Estimation of Shear Viscosity: Hydrodynamic and Configurational Study. *J. Chem. Phys.* **2019**, *151*, 104101.
(25) Weber, W.; Hünenberger, P. H.; McCammon, J. A. Molecular Dynamics Simulations of a Polyalanine Octapeptide under Ewald Boundary Conditions: Influence of Artificial Periodicity on Peptide Conformation. *J. Phys. Chem. B* **2000**, *104*, 3668−3675.
(26) Streitz, F. H.; Glosli, J. N.; Patel, M. V. Beyond Finite-Size Scaling in Solidification Simulations. *Phys. Rev. Lett.* **2006**, *96*, 1−4.
(27) Alder, B. J.; Wainwright, T. E. Phase Transition in Elastic Disks. *Phys. Rev.* **1962**, *127*, 359−361.
(28) Koishi, T.; Yasuoka, K.; Ebisuzaki, T. Large Scale Molecular Dynamics Simulation of Nucleation in Supercooled NaCl. *J. Chem. Phys.* **2003**, *119*, 11298−11305.
(29) Swope, W. C.; Andersen, H. C. 106-Particle Molecular-Dynamics Study of Homogeneous Nucleation of Crystals in a Supercooled Atomic Liquid. *Phys. Rev. B: Condens. Matter Mater. Phys.* **1990**, *41*, 7042−7054.
(30) Lemarchand, C. A. Distribution of Melting Times and Critical Droplet in Kinetic Monte Carlo and Molecular Dynamics. *J. Chem. Phys.* **2013**, *138*, 034506.
(31) Hardy, W. H.; Crawford, R. K.; Daniels, W. B. Experimental Determination of the P−T Melting Curve of Argon. *J. Chem. Phys.* **1971**, *54*, 1005−1010.
(32) Roder, H. M. Institute for Basic Standards *Liquid Densities of Oxygen, Nitrogen, Argon and Parahydrogen (Metric Supplement)*; U. S. Department of Commerce, National Bureau of Standards: Washington, D.C., 1974, p 109.
(33) Van Witzenburg, W. Density of Solid Argon at the Triple Point and Concentration of Vacancies. *Phys. Lett. A* **1967**, *25*, 293−294.
(34) Lechner, W.; Dellago, C. Accurate Determination of Crystal Structures Based on Averaged Local Bond Order Parameters. *J. Chem. Phys.* **2008**, *129*, 114707.
(35) Tsuchiya, Y.; Hasegawa, H.; Iwatsubo, T. Prediction of the Melting Point of N-Alkanes Using the Molecular Dynamics Method. *J. Chem. Phys.* **2001**, *114*, 2484−2488.
(36) Luo, S.-N.; Strachan, A.; Swift, D. C. Vibrational Density of States and Lindemann Melting Law. *J. Chem. Phys.* **2005**, *122*, 194709.
(37) Forsblom, M.; Grimvall, G. Homogeneous Melting of Superheated Crystals: Molecular Dynamics Simulations. *Phys. Rev. B: Condens. Matter Mater. Phys.* **2005**, *72*, 54107.
(38) Delogu, F. Cooperative Atomic Displacements and Melting at the Limit of Superheating. *J. Phys. Chem. B* **2006**, *110*, 3281−3287.
(39) Abraham, M. J.; Murtola, T.; Schulz, R.; Páll, S.; Smith, J. C.; Hess, B.; Lindahl, E. GROMACS: High Performance Molecular Simulations through Multi-Level Parallelism from Laptops to Supercomputers. *SoftwareX* **2015**, *1−2*, 19−25.
(40) Bussi, G.; Donadio, D.; Parrinello, M. Canonical Sampling through Velocity Rescaling. *J. Chem. Phys.* **2007**, *126*, 014101.
(41) Berendsen, H. J. C.; Postma, J. P. M.; van Gunsteren, W. F.; DiNola, A.; Haak, J. R. Molecular Dynamics with Coupling to an External Bath. *J. Chem. Phys.* **1984**, *81*, 3684−3690.
(42) Flubacher, P.; Leadbetter, A. J.; Morrison, J. A. A Low Temperature Adiabatic Calorimeter for Condensed Substances. Thermodynamic Properties of Argon. *Proc. Phys. Soc.* **1961**, *78*, 1449−1461.
(43) Dodge, Y. *Chi-Square Goodness of Fit Test BT—The Concise Encyclopedia of Statistics*; Springer New York: New York, NY, 2008; pp 72−76.
(44) Nauchitel', V. V. Energy Distribution Function for the NVT Canonical Ensemble. *Mol. Phys.* **1981**, *42*, 1259−1265.
(45) Scalas, E.; Gabriel, A. T.; Martin, E.; Germano, G. Velocity and Energy Distributions in Microcanonical Ensembles of Hard Spheres. *Phys. Rev. E: Stat., Nonlinear, Soft Matter Phys.* **2015**, *92*, 022140.
(46) Kneller, G. R.; Hinsen, K. Quantitative Model for the Heterogeneity of Atomic Position Fluctuations in Proteins: A Simulation Study. *J. Chem. Phys.* **2009**, *131*, 045104.
(47) Julin, J.; Napari, I.; Vehkamäki, H. Comparative Study on Methodology in Molecular Dynamics Simulation of Nucleation. *J. Chem. Phys.* **2007**, *126*, 224517.
(48) Turnbull, D.; Fisher, J. C. Rate of Nucleation in Condensed Systems. *J. Chem. Phys.* **1949**, *17*, 71−73.

https://doi.org/10.1021/acs.jpcc.1c10392
J. Phys. Chem. C XXXX, XXX, XXX−XXX